Mon. Not. R. Astron. Soc. **000**, 000–000 (0000) Printed 14 August 2015 (MN LATEX style file v2.2)

The NGC 4013 tale: a pseudo-bulged, late-type spiral shaped by a major merger

Jianling Wang[1,2⋆], Francois Hammer[3]†, Mathieu Puech[3], Yanbin Yang[3], Hector Flores[3]
[1]*Key Laboratory of Optical Astronomy, National Astronomical Observatories, Chinese Academy of Sciences*
[2]*National Astronomical Observatories, Chinese Academy of Sciences, Beijing 100012, China.*
[3]*Laboratoire GEPI, Observatoire de Paris, CNRS-UMR8111, Univ. Paris-Diderot, 5 place Jules Janssen, 92195 Meudon France.*

Received ; accepted

ABSTRACT
Many spiral galaxy haloes show stellar streams with various morphologies when observed with deep images. The origin of these tidal features is discussed, either coming from a satellite infall or caused by residuals of an ancient, gas-rich major merger. By modeling the formation of the peculiar features observed in the NGC 4013 halo, we investigate their origin. By using GADGET-2 with implemented gas cooling, star formation, and feedback, we have modeled the overall NGC 4013 galaxy and its associated halo features. A gas-rich major merger occuring 2.7 to 4.6 Gyr ago succeeds in reproducing the NGC 4013 galaxy properties, including all the faint stellar features, strong gas warp, boxy-shaped halo and vertical 3.6μm luminosity distribution. High gas fractions in the progenitors are sufficient to reproduce the observed thin and thick disks, with a small bulge fraction, as observed. A major merger is able to reproduce the overall NGC 4013 system, including the warp strength, the red color and the high stellar mass density of the loop, while a minor merger model can not. Because the gas-rich model suffices to create a pseudo-bulge with a small fraction of the light, NGC 4013 is perhaps the archetype of a late-type galaxy formed by a relatively recent merger. Then late type, pseudo-bulge spirals are not mandatorily made through secular evolution, and the NGC 4013 properties also illustrate that strong warps in isolated galaxies may well occur at a late phase of a gas-rich major merger.

Key words: Galaxies: evolution - Galaxies: spiral - Galaxies: individual: (NGC 4013) - Galaxies: interactions

1 INTRODUCTION

Mergers are important for galaxies formation and evolution in the concordance cosmological model. Semi-empirical simulations and observations have shown that about half local spiral progenitors have experienced a major merger process (mass ratio greater than 1:4) since $z \sim 1.5$ (Hammer et al. 2005, 2009a; Puech et al. 2012). The process of the disk rebuilding after a major merger has been extensively explored by modern state-of-art simulation (Robertson et al. 2006; Hopkins et al. 2009; Springel & Hernquist 2005; Hammer et al. 2010; Wang et al. 2012). Hopkins et al. (2010) using large set of simulations showed that the final disk fraction of major merger remnant is a function of mass ratio and gas fraction, although it shows a large scatter due to the merger orbital parameters (see their Fig. 7). For example, equal (or 3:1) mass merger can lead to a new spiral with bulge fraction lower than 28% (12%) as long as the gas fraction is higher than 80% (50%), respectively. Since high redshift galaxies have much higher gas fraction than local spirals (Rodrigues et al. 2012), this is consistent with the disk rebuilding scenario after a major merger (Hammer et al. 2005). The imprints of major merger events are easily and rapidly washed out in the center part of galaxies, because the density is high and the dynamical timescales are short. But at large scales, in the outskirts of galaxies, the density is low, and the dynamic timescales are expected to be relatively large, which can let imprints of the merger process lasting several Gyr. Then ancient major merger events should leave imprints in spiral halos, if many spirals have seen their disk rebuilt after a gas-rich major merger.

Deep observations by Martínez-Delgado et al. (2010) have revealed that many local spirals show faint tidal features in their halo (see e.g., M31 and NGC 5907) with diverse morphologies. These faint features have been formerly interpreted as evidence for minor mergers. However, an issue with this scenario is that the nucleus of the infalling galaxy is difficult to destruct. Such a residue is generally not observed, even though it is predicted by simulations (Martínez-Delgado et al. 2008, 2009): this is a clear weakness for the minor merger alternative.

Wang et al. (2012) have shown that the complex two loops in the halo of NGC 5907 can be well reproduced by a major merger

⋆ E-mail:wjianl@bao.ac.cn
† E-mail:francois.hammer@obspm.fr

model. Hammer et al. (2010) also modeled the M31 Giant Stream as being formed by tidal tail particles captured by the remnant of an ancient major merger. More modeling is needed to show that gas-rich major mergers can generate the various tidal features observed in local spiral halos, as it is predicted that about half local spirals have experienced such events (Hammer et al. 2009a; Puech et al. 2012).

In this paper, we use a gas rich major merger model for reproducing the loop and the other faint features observed in the halo of NGC 4013 as well as the overall structure of this edge-on spiral galaxy. Deep observations obtained by Martínez-Delgado et al. (2009) have revealed many faint features including a loop-like feature in the stellar halo of NGC 4013, which has been formerly interpreted as caused by a minor merger event despite the absence of any progenitor residue. Deep observations with Spitzer IRAC by Comerón et al. (2011, hereafter C11) have revealed that there is an extra flattened extended component in the vertical direction lying besides the thin and the thick disks. Such a component contains $\sim$ 20% of the total mass and C11 convincingly argued that it cannot be explained by an ongoing minor merger. Furthermore the HI map of NGC 4013 reveals a very prominent warp. The above motivated us to verify whether a major merger can reproduce all the peculiarities observed in NGC 4013, including the low bulge fraction, the loop system, the warp, and the extended vertical component.

This paper is organized as follows. In Section 2, we describe the basic properties of NGC 4013, and summarize the observed peculiar features. The simulation method and initial conditions are described in Section 3. The results are presented in Section 4. In the last Section, we discuss our results and summarize them.

2 NGC 4013 PROPERTIES

2.1 The NGC 4013 galaxy

NGC 4013 is an Sb type edge-on spiral (Buta et al. 2007), and there are thirteen redshift-independent distances available for this galaxy, ranging from 15.6 to 24.1 Mpc, with an average value of 18.6 Mpc. Using the baryonic Tully-Fisher relation, this results in a velocity $\sim$ 210 km/s, while the observed rotational velocity of NGC 4013 is about 177 km/s (McGaugh 2005), with a maximum velocity of 195 km/s (Bottema 1996). Therefore, we adopted a distance of 16.9 Mpc (Willick et al. 1997), which is consistent with the baryonic Tully-Fisher relation (McGaugh 2005; Puech et al. 2010) and within one sigma from the average distance calculated above.

There is a boxy bulge component that is thought to be a bar or the result of a merging event (Athanassoula & Misiriotis 2002; Binney & Petrou 1985). There are different estimates of the bulge fraction in the literature. Bianchi (2007) used a radiative transfer model to decompose the V and K' band images into a stellar disk, bulge, and dusty disk to account for extinction. We considered only B/T determination in NIR bands to avoid the strong extinction associated to an edge-on galaxy. Bianchi (2007) found that the bulge fraction is 27% in K band by fixing the Sérsic index of the bulge component to 4. McDonald et al. (2009), using one-dimension fitting in K band, found a value of only 1%. The S4G project[1](Sheth et al. 2010) has released the result of two components fitting on Spitzer IRAC 3.6 μm images with a Sérsic bulge and an exponential disk. In their result, the bulge fraction is about 9%. We fitted the Spitzer IRAC 3.6 μm image with different components using GALFIT 3 (Peng et al. 2010). For comparison with C11, we used similar components except we added one bulge profile. In our fitting, one Sérsic bulge, two edge-on disks, and one exponential component for the stellar halo are used. We found that the bulge, thin disk, thick disk, and stellar halo fractions are 4%, 25%, 53%, and 19%, respectively.

The thick disk is about a factor 2.12 larger than the thin disk. This fraction agrees with C11, who found that the thick disk is 1.2 – 2.2 larger than the thin disk, and that the extended component contains 20% to 26% of the total mass without considering the bulge component. We found that the Sérsic index of the bulge is 0.12, indicating that the bulge of NGC 4013 is a pseudo bulge. The disk scalelength of our fitting is 2.11 kpc for both the thin and thick disks, which is comparable to Saha et al. (2009) who got a value 2.3 kpc by fitting the Spitzer IRAC 4.5 μm image. We notice that the optical scalelength is larger than the infrared one, which is found to be 3.24 kpc (van der Kruit & Searle 1982; Martínez-Delgado et al. 2009).

The total stellar mass was estimated following Wang et al. (2012) using M/L-color relation from Bell et al. (2003) with the 2MASS K_s band and B-V color from NED after correcting for Galactic extinction. A ″diet″ Salpeter IMF was assumed. Then we get that the stellar mass of NGC 4013 is about 4.4×10^{10} $M_\odot$. The HI mass is about 2.8×10^9 $M_\odot$ from Bottema (1996) and the H2 mass is about $1.9\times10^9 M_\odot$ from Gomez de Castro & Garcia-Burillo(1997). This leads to a total gas mass of about 6.6×10^9 $M_\odot$ after considering a 40% He contribution (Just et al. 2006), and a total gas fraction of 13%.

2.2 Peculiar features of the NGC 4013 halo

From its mass and gas content NGC 4013 has been considered as a galaxy relatively similar to the Milky Way (Martínez-Delgado et al. 2009, hereafter MD09). However, observations show that NGC 4013 is very different from the Milky Way in many aspects:

- There is a ”prodigious” HI warp starting at the optical edge of NGC 4013, which is one of the largest warps ever observed (Bottema et al. 1987; Bottema 1996, 1995);
- A giant loop-like stellar stream was found by MD09, among the brightest one ever observed (Martínez-Delgado et al. 2008);
- A box-shaped outer ”stellar halo” (larger than 15 kpc) was also found surrounding the galaxy (MD09), together with four faint tidal features;
- C11 identified a massive extended halo component, which contains about 20%-26% of the total mass. The mass of the thick disk is about 1.2 to 2.2 times larger than the thin disk, contrasting with the Milky Way, for which this ratio is only 0.21 (Read et al. 2008).

2.3 Brightness and red color of the NGC 4013 loop

The observed mass surface density of the loop can provide useful constraints on the model. MD09 measured a B-R color of $1.6^{+0.6}_{-0.4}$, and $\mu_R = 27.0^{+0.3}_{-0.2}$. With these numbers one can derived the mass surface density for the loop structure, which is $\Sigma_\star = 1.42^{+4.13}_{-0.93}$ $M_\odot$ pc^{-2}.

The B-R color of the main loop and associated tidal features is 1.5 after accounting for Galactic extinction and k-correction. It corresponds to an old metal-rich stellar population, intermediate between that of elliptical (B-R= 1.62) and lenticular (B-R= 1.43)

[1] http://www.oulu.fi/astronomy/S4G_PIPELINE4/MAIN/index.html#entry1003

galaxies (see Table 3 of Fukugita et al. 1995). Comparing to observed galaxies, it is indeed redder than what is found for field S0 galaxies after accounting for Galactic extinction and k-correction (Barway et al. 2005).

Let us consider that the loop can be either related to a massive progenitor or alternatively to a red dwarf elliptical. It is ∼ 0.6 mag redder than the Sagittarius stream (Martínez-Delgado et al. 2004). This challenges the stream origin as an old, metal poor stellar population related to dwarf ellipticals. From its derived stellar surface density, the NGC4013 loop is 1.6 mag brighter than the NGC5907 loops and 4 mag brighter than the Sagittarius stream. The above strengthens our motivation to model it as resulting from a prominent tidal tail caused by an ancient major merger, and linked to old and metal-rich stars commonly found in massive galaxies. At the same time, we aim to also investigate whether such a major merger is able to explain the strong warp, the boxy halo, and the extended component.

3 SIMULATIONS AND INITIAL CONDITIONS

We use the parallel TreeSPH code GADGET-2 (Springel 2005), in which both energy and entropy are conserved. Cooling, star formation, and feedback processes of the interstellar medium (ISM) were implemented as in Wang et al. (2012), which follow the prescription described by Cox et al. (2006) and Springel (2000). Here we give brief introduction of the method (see Wang et al. 2012 for more details). Radiative cooling is important for gas to cool down to the central region of the dark halo and then form stars. The cooling rate is calculated following Katz et al. (1996), in which the gas is treated as a primordial plasma and the ionization states of H and He and collisional ionisation equilibrium are assumed. During the simulation, gas particles in these dense regions can form stars, and the star formation rate of each gas particle is calculated according to Kennicutt-Schmidt law ($\frac{d\rho_\star}{dt} \propto \rho_{gas}^{1.5}$, ρ standing for local gas density, see Kennicutt 1998). As stars form, gas is transformed into collision-less matter using a stochastic technique (Springel & Hernquist 2003). Supernova feedback is associated with star formation and is crucial for the stability of the simulations and regulating star formation. The energy from supernovae is deposited into the ISM. This energy heats and pressurizes the gas, and stabilizes it from further gravitational collapse. The feedback energy can also be thermalized, which is controlled by the time scale of this process and the equation of state.

The initial conditions were set up similarly to Wang et al. (2012), except that we scaled down the scalelength of the two merger progenitors by a factor two to account for the size evolution with redshift (Franx et al. 2008; Wuyts et al. 2010). This scaling factor is consistent with a later-type galaxy size evolution relation (van der Wel et al. 2014, see Table 1). Progenitors are 60% − 70% gas-rich spirals, which is reasonable for z=1.5-2 galaxies (corresponding to 9 Gyr ago, see Rodrigues et al. 2012). We used the same initial baryonic fraction (f_{bar} = 9%) and progenitor density profiles that what was adopted by Wang et al. (2012).

Cosmological simulations provide constraint on the orbital parameters. The pericenter and eccentricity are chosen to be following Khochfar & Burkert (2006). Briefly, we estimated the virial radius of the primary galaxy halo at the time of merger occuring (∼ 7 Gyr ago) to be about 114 kpc, following the relationship between the virial radius and total mass derived from cosmological simulations (Springel & White 1999). The pericenter used in our simulations was larger than ∼ 23 kpc. Then the ratio between pericenter and virial radius is 0.20 and the eccentricity is larger than 0.86, which satisfies the cosmological constraints (Khochfar & Burkert 2006).

We choose for the primary galaxy a retrograde and closed to polar orbit, and for the secondary galaxy a prograde and inclined orbit. A retrograde orbit is favorable for an efficient disk rebuilding (see e.g., Hammer et al. 2010), and well-suited to NGC 4013, which is a spiral with small bulge component. The prograde orientation of the secondary is favorable for generating long tidal tails (Wang et al. 2012; Hopkins et al. 2009; Toomre & Toomre 1972; Barnes & Hernquist 1992).

Given the large parameter space, we acknowledge not having been able to thoroughly examine all possible configurations. However, thanks to the above constraints, the searching parameter space can be significantly reduced. In our former work (Wang et al. 2012), the theory of the tidal tail particles motion in galaxy potential have been extensively explored, which help optimize the searching parameter space. During the searching process, we first use low resolution simulation with a few hundred thousand particles to primarily find the possible geometry. This primary search was done in a large coarse grid of parameters consisting of pericenter distance, eccentricity of orbit, and inclination angles for these two interacting galaxies. After getting the possible parameters, we finely tune the parameters around this point with one or two million particles. We confirmed that the results between low and high resolution simulations show little differences, except the later leads to a better definition of the loop and tidal tail features. The softening length adopted in low resolution for dark matter, gas, star particles are, 0.3 kpc, 0.15 kpc, and 0.1 kpc. In general, increasing particles number N allows the gravitational softening length to be decreased with increasing computational time (Cox et al. 2006). We have tested the softening effect by decreasing softening length for some high resolution simulations as shown in Table 1, and the results do not differ too much. This indicates that our simulations are converging well. We found that a series of models in a family of a parameters with pericenter between 23 kpc and 27 kpc, and eccentricity of orbit between 0.9 and 0.93, can produce the overall NGC4013 (see Table 1). There is a degeneracy in the models of NGC 4013 similar to that NGC 5907 (Wang et al. 2012), which is the loop order can not be identified based on current observations. Further deep observations are need to definitively break this degeneracy (see the following section).

4 RESULTS

4.1 Loop formation during the merger

Wang et al. (2012) described the basic properties of loop systems formed after a major merger, which have lead to successfully model NGC 5907 and of its two loops structures. Hammer et al. (2013) demonstrated that the dSphs in the M31 disk of satellites are spatially distributed along a similar system of loops. In this paper, we use the loop properties to model the tidal features observed in NGC 4013.

The top two rows of Figure 1 show the stellar distribution of a 1:3 major merger. In the 4.5 Gyr panel, the first tidal tail is generated after the first passage, as indicated by a yellow arrow. The second tail is formed before fusion at 4.7 Gyr and is indicated by a black arrow. This tidal tail will generate the loop observed in NGC 4013. The first loop forms at 5.4 Gyr and is shown by a red arrow. It is followed by the second, third, and fourth loops, which are shown in the 6.9 Gyr panel and are labeled by a purple, a blue, and a light

blue arrow, respectively. At 7.4 Gyr the fifth loop (labeled by a green arrow) is formed and resemble what we observed in NGC 4013. As shown by Wang et al. (2012) the loops become larger hence fainter with time. The loop system can be maintained during at least 9.3 Gyr. To better illustrate how the loops formed through potential captured from tidal tail particles, we isolated them and traced their motions in Fig. 2.

The loop formation mechanism is similar to that described in Wang et al. (2012). New loops are continuously fed by falling particles with time, while low order loop become fainter, which make them more difficult to be detected than high order loops.

Since the loops appear consecutively, from low order to high order with different surface brightnesses (or mass) densities, it helps identify the one matching the observations. Meanwhile, tuning the initial position angle of the primary galaxy control the final disk position relative to a given order loop. The phase angle of the different loops are close to 90 degrees (Wang et al. 2012), so generally we just needed to rotate the disk by 180 degrees to have the loop and disk geometry matching observation for a given loop order. For details about the loop formation and properties, refer to Wang et al. (2012).

In Fig. 3, we show different loop orders formed by particles falling back onto the remnant, which show geometrical resemblance with the observations. Four different models, M3R23M2, M3R23M1G7, M3R26M2A, and M3R27M2 are used to produce these different loop orders at the different times. The loop order and the observed time are labeled at top of each panel. Each panel shows a mass surface density that is limited by the observed loop density, i.e., $\Sigma_\star = 0.5\ M_\odot pc^{-2}$. From current observations, it is difficult to judge what is the loop order that best fits the observations because we need more constraints on their formation time. This is similar to that was found by Wang et al. (2012).

The two bottom rows of Figure 1 show the distribbution of the gaseous phase during the merger process. At 6.9 Gyr there is formation of a strong warp induced by the merger, which becomes stronger with time. At 7.4 Gyr and 9.3 Gyr it persists and resembles the observed one. The warp of NGC 4013 is one of the strongest observed one (Bottema et al. 1987), which indeed suggests a not too ancient, violent merger event.

4.2 Box-shaped feature formed by particles falling back from the same tidal tail

MD09 (see their Figure 3) identified a huge, at least 3′(∼15kpc) sized box-shaped in the outer stellar halo, which they called feature B. The loop-like feature (C for MD09) starts at the northeast corner of the boxed-shaped halo, and ends at the southeast corner of the box. There is also a pair of wings, one at the northwest direction (E) and a more extended one (D) is at the southwest. Here we show that the box-shaped stellar halo and the four wings out of the disk are a natural product of single major merger model, and are all coming from the same system of tidal tails.

Fig.2 shows stellar particles from the tidal tails only, at different epochs. After their capture, stellar particles move along loops that are mostly lying in a single plane, though it thickness can be affected by precession. The second and fourth panels of Fig.4, we show their projected surface mass density, at 7.4 Gyr and 9.5 Gyr. It reveals a clear X-shaped surface density that is predicted in our model because tidal tail particles are coming from 4 directions drawn by the two almost symmetric loops seen in the 7.4 Gyr panel of both Figures 1 and 2. The X-shaped feature persists for several Gyr as loops and is similar to what was found by Purcell et al. (2010). The huge box-shaped stellar halo in NGC 4013 results from the accumulation of particles surrounding the X-shaped feature (see contours in Fig.4, third panel). Then our modeling naturally explains the box-shaped halo (B), the loop (C) and the pair of wings lying west of the disk (D and E features for MD09).

As explained and detailed in Wang et al. (2012), the high order loops are made of material coming originally from the inner region of the progenitors compared to low order one, they are associated with larger stellar mass surface densities. This property suffices to explain the relatively high surface brightness of the boxy halo as well as that of the loop if those correspond to high order loop particles, i.e., with a relatively recent merger. In the next subsections we verify whether this is consistent with other observations of NGC4013.

4.3 Strong gas warp generated by the major merger process

Due to the dissipational properties of the gas, the gas motions in the halo are rapidly decoupled from stellar streams (see Figure 1). Most major merger events result in gas warps, which can last for several Gyr as shown in Fig.1. The angular inclination of the massive progenitor has been set close to polar, and with a retrograde orbit this results in a very strong gas warp. Fig. 5 shows a comparison between the observed HI gas morphology from Bottema (1996) with the simulation for which only cold gas ($T < 20,000K$) is shown.

Observations show that the gas fraction of NGC 4013 is about 13%. After turning the feedback strength down after fusion (Wang et al. 2012; Hammer et al. 2010) to allow a new disk to reform after the major merger, most of the gas is consumed and converted into stars. This results in a gas fraction between 14% and 16% for most models, which matches well the observed range (see Tab. 1).

4.4 The NGC4103 disk rebuilt after the major merger

As shown in Section 2, NGC 4013 has a pseudo-bulge (Kormendy & Kennicutt 2004) with a very small B/T value. To check whether a newly rebuilt spiral galaxy is consistent with NGC4013, we analyzed the mass surface density in the simulation as it was done in Wang et al. (2012). A Sérsic bulge and two exponential disk components were fitted, while the central region, which is dominated by the softening was excluded. Fig.6 shows the fit for model M3R24M2, and the fitting results are listed in Table 1. In this model a small bulge fraction is obtained with B/T ∼ 25% and with a Sérsic index of 1.37. By increasing the initial gas fraction to 70%, see model M3M1G7, the B/T ratio decreases to 14%. All the models listed in Table 1 show bulge Sérsic indices smaller than 1.7, which are consistent with pseudo-bulges (Kormendy & Kennicutt 2004). The disk scale-length in our model fitting is about 2.8 kpc, which is close to that observed.

4.5 Rotation curve

We checked whether the rotation curve predicted by the model matches the observed one. In Fig. 7, the observational data are taken from Bottema (1996), while the model rotation curve is calculated assuming a rotating disk at equilibrium ($V_c = \sqrt{\frac{GM(<r)}{r}}$, Wang et al. 2012). At r < 10 kpc, the rotation curve of the model agrees well with observations. From 10 to 20 kpc (as indicating by two arrows), the observed rotation curve falls down dramatically, which is due to impact of the strong warp.

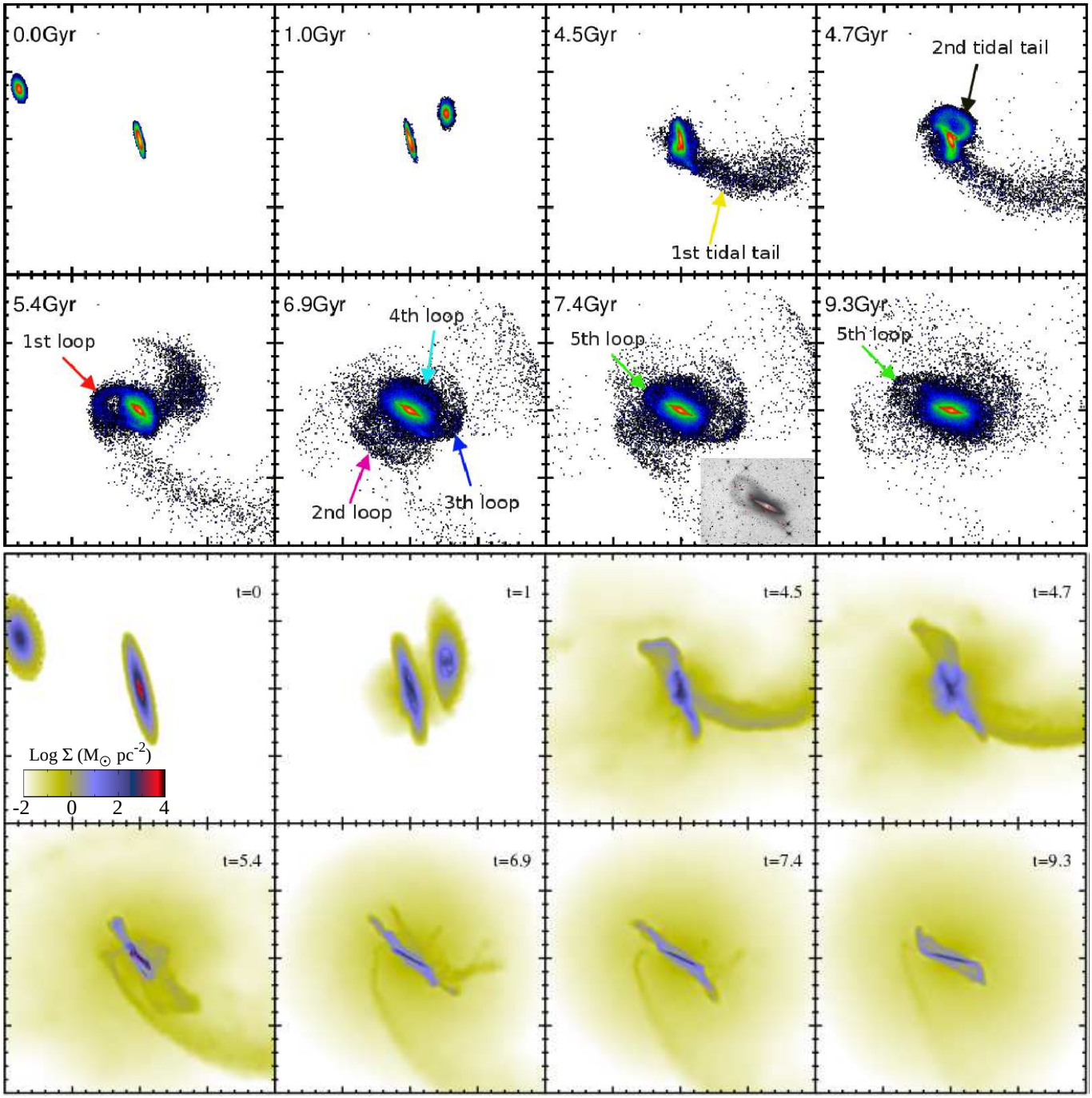

Figure 1. Star and gas particles distributions for a merger with mass ratio 1:3 (model M3R24M2) at different epochs. Star particles are shown in the top two rows. The best fit to observations is at 7.4 Gyr, at which the structure and over-density of the fifth loop also match the observations, and the observed image from Martínez-Delgado et al. (2009) is shown at the right bottom of this panel. The gas surface density is shown in the bottom two rows. The size of each panel is 200 by 200 kpc and the arrows are explained in the text.

4.6 Vertical Profile

By fitting a vertical luminosity profile on the Spitzer IRAC 3.6μm image, C11 found that NGC 4013 can not be fitted satisfactorily by a canonical thin+thick disk structure. Instead, they found evidence that there are a thin and a thick disk and an extra flattened component, which contains ∼ 20% of the total mass. Fig.8 compares our simulation model with the observed vertical profile from Comerón et al. (2011). To measure the vertical mass surface density, we have selected the same physical radius chosen by Comerón et al. (2011), namely $-0.5r_{25} < R < -0.2r_{25}$, with $r_{25} = 147''$. To convert stellar mass into 3.6μm light, we used a stellar mass to light ratio M/L of 0.85 from Meidt et al. (2014) by assuming a 'diet' Salpeter initial mass function (Eskew et al. 2012). To account for uncertainties, we adopted a range of 0.5-1.5 on M/L.

Fig.8 shows the result. The simulation (red curve) matches the observations all the way from z=20 to 120″ predicting well the presence of the extra component. The red curve corresponding to

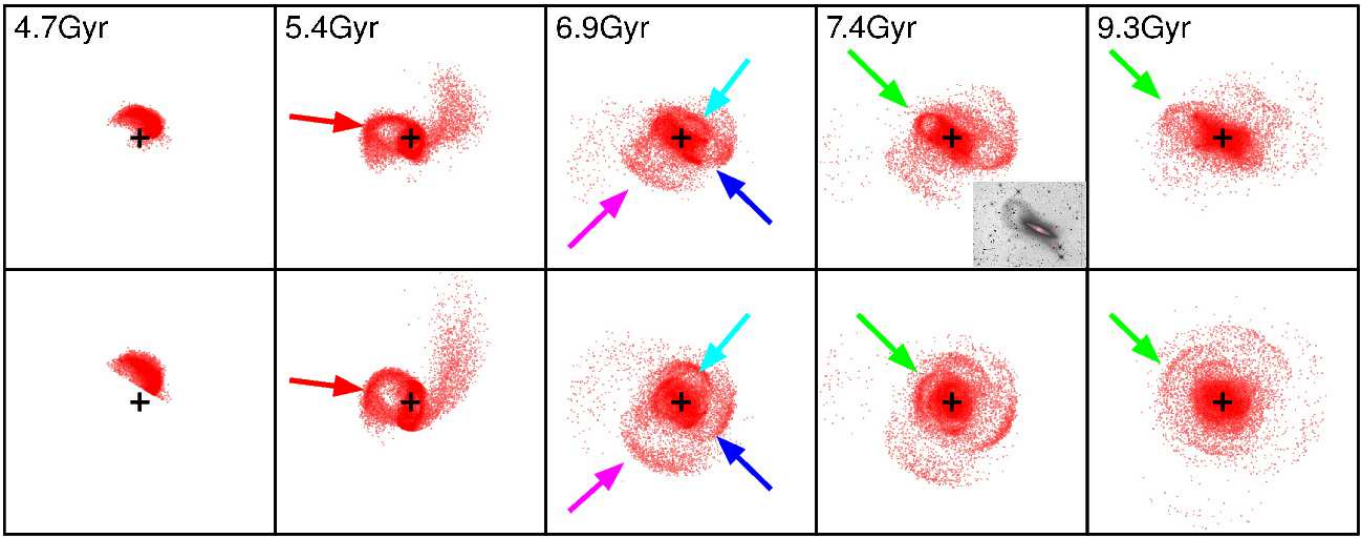

Figure 2. Loops formed by the second tidal tail for model M3R24M2. Only particles in the tidal tail are shown here. The top row shows the loops formation process at the viewing angle matching NGC 4013. The loop at 7.4 Gyr resembles that of NGC 4013, while according to its brightness the loop at 9.3 Gyr is only marginally consistent with the observed one. The bottom row shows the same data with a face-on view. At 5.4 Gyr, the red arrow shows the first loop formed. The second, third, and fourth loop are formed at 6.9 Gyr indicated by purple, blue, and light blue arrows, respectively. The fifth loop, which resembles observation at 7.4 Gyr is labeled by a green arrow as well as in the 9.3 Gyr panel. Observed image is overlaped at the 7.4 Gyr panel.

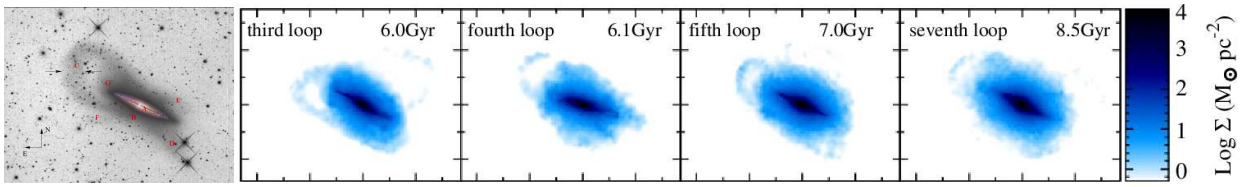

Figure 3. Comparison between the observation predictions of different order loops formed at different time. The left panel is observed image (Martínez-Delgado et al. 2009), while the right four panels are from simulation. The surface mass density is cut at $\Sigma_\star = 0.5(M_\odot\ pc^{-2})$, which corresponds to the 1σ limit of loop surface mass density. The high order loop appears much later compared to those of low order. The size of each panel is ~ 82 by 62 kpc. Models used from left to right are M3R23M2, M3R23M1G7, M3R26M2A, and M3R27M2.

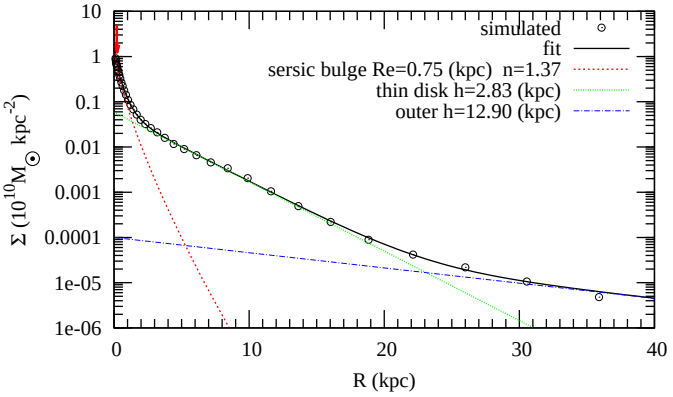

Figure 6. Surface brightness mass density distribution as a function of radius for model M3R24M2. In the fitting Sérsic bulge and exponential disk components are used. Black open circles indicate the simulation results and the black line shows the fitting result. Different components are shown using different color lines. The red arrow (just above Σ=1 and R<< 1 kpc) indicates two times values of the softening length, which is very small when compared to the bulge characteristic size. Then the softening does not affect the result.

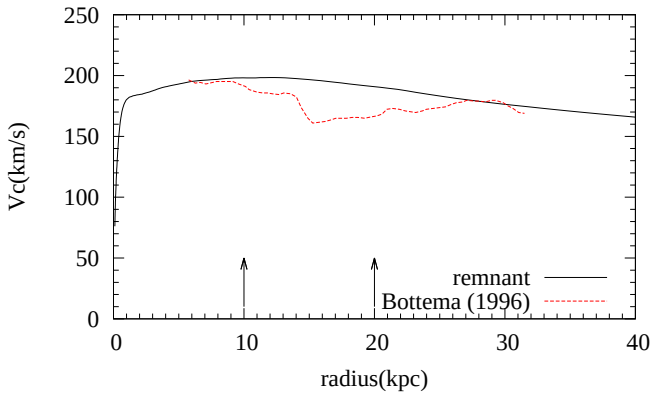

Figure 7. Comparison between the rotation curves of the simulated galaxy after the major merger (black line, model M3R24M2 at 7.4 Gyr) and observation (red dashed line). The observation rotation curve is from Bottema (1996). The rotation curve of the simulation is calculated by simply using the mass model, with $V_c = \sqrt{\frac{GM(<r)}{r}}$.

a mass-to-light ratio of 0.85 at the inner region under-predicts the observations, which might be related to a change in M/L between

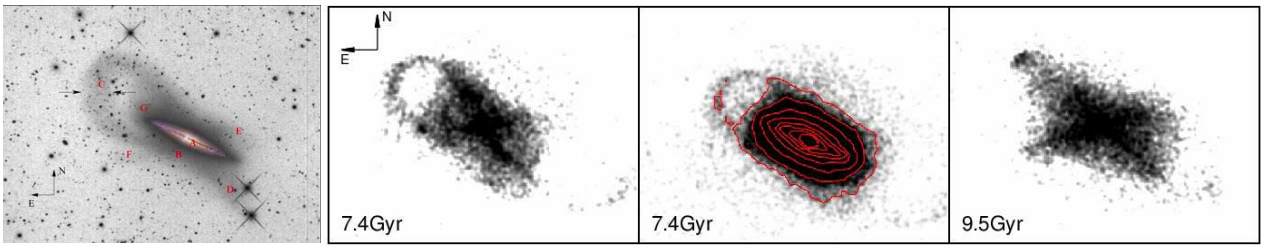

Figure 4. The left panel show observed image from Martínez-Delgado et al. (2009), and the right three panels show results from simulation. Box-shaped feature formed by the coming back particles in the tidal tail of model M3R24M2. Here the contrast is tuned to clearly view the X-shaped morphology. In the second and right panels, the particles are selected by isolating tidal tail particles after the formation of the second tidal tail, and tracing their motions to 7.4 Gyr and 9.5 Gyr. The X-shaped features is not a transient feature but would require deep color image to be detected. It generates the box-shaped stellar halo and a pair of (observed) wings features west and southwest. In the third panel all particles are shown with contours overlapped to evidence the box-shaped feature in the stellar halo resulting from the tidal tail particles. The size of each panel is ~ 82 by 62 kpc.

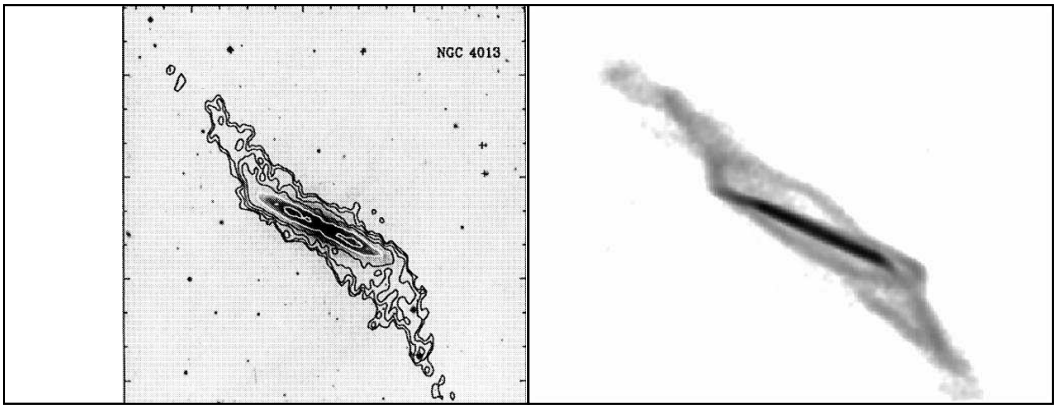

Figure 5. Comparison between the observed gas morphology with that from the simulation. In the left panel the contours show the observed HI map superimposed on the optical image (from Bottema 1996), and the right panel shows the simulated mass density of cold gas from model M3R24M2. The size of each panel is ~ 82 by 62 kpc.

the different structures (see e.g., the green curve that matches the observations near the inner region).

5 DISCUSSION AND CONCLUSION

We modeled NGC 4013 as resulting from a 3:1, gas-rich major merger. The NGC4013 loop and other tidal features can be explained by stellar streams, which are natural and persistent residuals of such mergers. The model suggests that tidal tails stars were captured by the gravitational potential of the remnant, and formed a loop system that have lifetimes maximized by the absence of dynamical friction. The models also predict a newly formed disk and a small bulge, which show many similarities with the observed ones. It also reproduces well the distribution of stars at the outskirts, including the box-shaped halo and the light profile along and perpendicular to the disk. The merger event predicts a strong gas (HI) warp, which is spatially well decoupled from the old stars, as observed. With our modeling the above observed features can be reproduced all together if the merger occurred 2.7 to 4.6 Gyr ago, with a first passage occurring about 3.5 Gyr earlier.

The deepest image available for NGC 4013 is a combination of four images within different filters. This combined image results from various stellar populations and is also affected by dust extinction, which hampers a proper comparison with simulations, for which the stellar mass is the most reliable quantity. As the near infrared imagery traces better the stellar mass, we prefer to compare our simulation with near infrared data. In Fig. 9 we show the deep optical observations, the IRAC 3.6 μm image, and the simulation, together (compare panels (a) and (c), with panels (d) and (e), respectively). The mass surface density of the simulation was cut at the surface brightness limit of the observations. The deep IRAC observations show the presence of a thick disk and of an extended stellar halo. It does not show the loop simply because it is not deep enough to recover it.

An important role of major mergers in the past history of spiral galaxies is expected from observations of their progenitors, 6 Gyr ago (Hammer et al. 2005, 2009a), and empirically based Λ-CDM calculations of the merger rate (Hopkins et al. 2010; Puech et al. 2012). If galactic disks can be rebuilt after gas-rich mergers, it is quite natural that they may produce strong warps, tidal loop systems of old stars, and extended halo components. This paper presents the first ever made simulation reproducing successfully the overall properties of NGC4013. Previously, MD09 had superimposed a model aimed at reproducing the Monoceros Stream on NGC4013 revealing geometrical similarities. MD09 however noticed that a more massive progenitor was required to reproduce the NGC 4013 loop system.

Perhaps the most difficult challenge for a minor merger scenario is the elliptical-type color ($B - R = 1.6^{+0.6}_{-0.4}$) of the NGC 4013 loop: it is ~ 0.6 mag redder than metal poor, old stars that populate dwarfs or dwarf streams. For example dSphs show B - R $\leqslant$ 1, even for those dominated by old-stars (e.g., UMi,

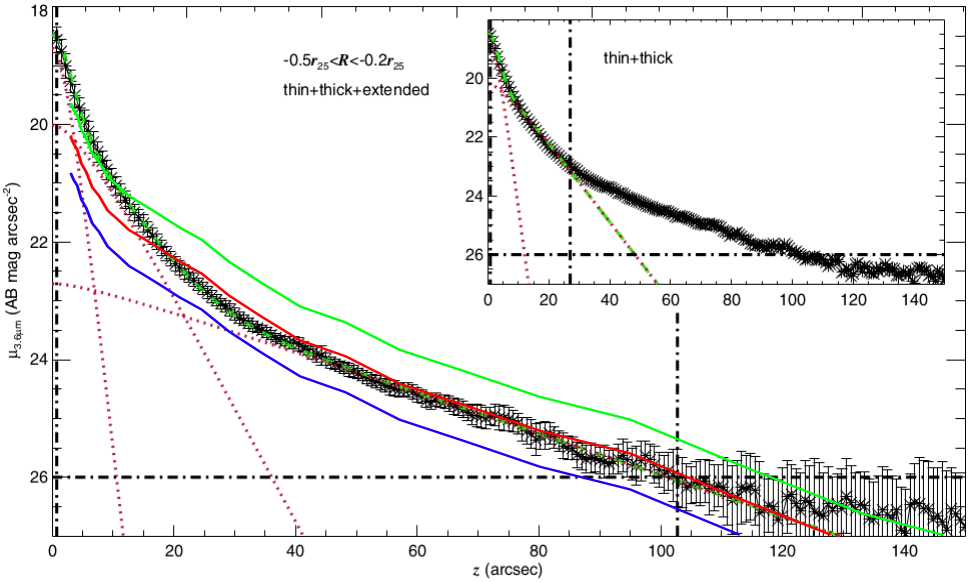

Figure 8. Comparison between the observed vertical 3.6μm luminosity profile with simulations (model M3R24M2). The solid color lines from simulations are overlapped on Figure 3 of Comerón et al. (2011). The red solid line shows results from simulations by assuming mass to light ratio 0.85 (Meidt et al. 2014). The green and blue solid lines show profiles with different mass to light ratio of 0.5 and 1.5, respectively while the M/L=0.85 reproduces well the extended halo component, it might need M/L=0.5 for fitting both disks.

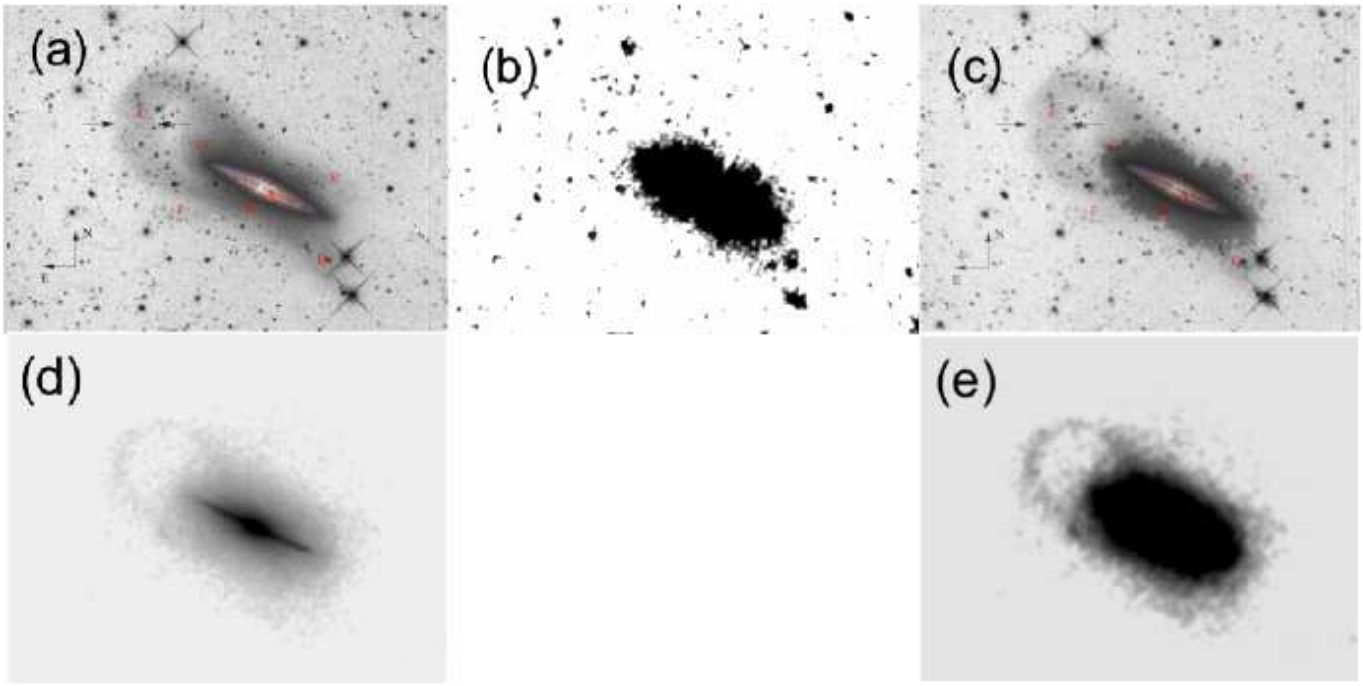

Figure 9. Comparison between observations and simulations. Panel (a) shows deep observations at optical wavelengths from MD09, revealing clearly the loops and other faint features. Panel (b) shows observations with Spitzer IRAC 3.6μm evidencing the thick disk and the stellar halo while the loop and other features are too faint to appear. Panel (c) shows combination of (a) and (b), which trace the stellar mass distribution less affected by dust extinction effects. Panel (d) shows the simulation of model M3R24R2 with very high contrast showing mostly the bulge, the thin disk and at fainter levels, the loop and the extended halo. Panel (e) shows the same model as (d) with a cut at a lower isophotal level showing the overall halo. The mass surface density of the simulation has been cut at the lower limit of the observed loop. The size of each panel is ~ 82 by 62 kpc.

Table 1. Parameters of the six models used in this study. Feedback model: high feedback as in Cox et al. (2006) is used before fusion, and changed to low feedback after fusion. Bulge Sérsic index *n* and disk scale-length are obtained by fitting the surface brightness density distribution with a Sérsic profile and two exponential functions.

parameters	M3R23M2	M3R24M2	M3R26M2A	M3R27M2	M3R23M1G7
mass ratio	3	3	3	3	3
Gal1 incy	-100	-105	-100	-100	-100
Gal1 incz	-130	-130	-130	-130	-130
Gal2 incy	-70	-70	-70	-70	-70
Gal2 incz	30	30	30	30	30
Gal1 gas fraction	0.6	0.6	0.6	0.6	0.7
Gal2 gas fraction	0.6	0.6	0.4	0.4	0.7
r_{peri} (kpc)	23	24	26	27	23
eccentricity	0.93	0.93	0.9	0.9	0.93
$N_{particle}$	2.0M	2.0M	2.0M	2M	1M
m_{dm}:m_{star}:m_{gas}	4:1:2	4:1:2	4:1:2	4:1:2	4:1:2
softening(ϵ_{dm}:ϵ_{star}:ϵ_{gas})(kpc)	0.3:0.1:0.15	0.3:0.1:0.15	0.24:0.08:0.12	0.24:0.08:0.12	0.3:0.1:0.15
Observed time (Gyr)	7.2	7.4	7.0	8.5	6.1
Thin disk scalelength(kpc)	2.83	2.83	2.72	2.81	2.56
Bulge sersic index(*n*)	1.64	1.37	1.32	1.10	0.81
Re of bulge (kpc)	0.88	0.75	0.83	0.91	0.78
B/T	23%	25%	21%	21%	14%
Final gas fraction	14%	14%	16%	16%	28%

Martínez-Delgado et al. 2001 and Sculptor, Hurley-Keller et al. 1999). The NGC 4013 loops and halo are perhaps an extreme illustration of previous findings (Mouhcine et al. 2006; Zibetti et al. 2004) that stellar haloes of most spiral galaxies (but the MW, see Hammer et al. 2007) are too red to be inhabited by metal-poor stars related to dwarfs.

It could be argued that a minor merger is still plausible, if some systematics affect the color measurement of a low surface brightness structure such as the NGC 4013 loop (but see MD09). If correct, the minor merger scenario has also to account for the much larger stellar mass surface density than what is found in tidal tails of dwarfs. Moreover a dwarf infall could explain neither the strong warp, the boxy-shaped halo or the vertically extended component. For those one would have to invoke independent origins, for example cooling gas for the warp (e.g., Radburn-Smith et al. 2014) and a 10:1 merger for the halo (e.g., C11 and see Figure 1 of Purcell et al. 2010). Adding this to the fact that the supposed dwarf residual is not seen in the deepest images as could be expected (see the discussion in Wang et al. 2012), a merger of satellite appears very unlikely for interpreting the NGC 4013 system.

Wang et al. (2012) tested the range of more massive minor (or intermediate) merger (from 15:1 to 10:1) for reproducing the NGC 5907 system, using characteristic times similar to NGC 4013. They estimated that 12:1 is a limit for reproducing NGC 5907 with orbital parameters as expected from cosmological simulations, and this agrees with predictions from Hopkins et al. (2009) for the formation of massive spirals. However, if a $\sim$ 10:1 merger may explain the box-shaped halo (Purcell et al. 2010), it could not account for the red color of the NGC 4013 loop.

This leaves a major merger as the only possible alternative. NGC 4013 also appears to show quite exceptional properties when it is compared to other edge-on spiral galaxies. In C11, it is one of the two (among 46) galaxies showing an extra vertical component to the thin and thick disks. It is also the only one (among seven) showing an extended vertical dust distribution above the disk, which has been detected by *Herschel* (Verstappen et al. 2013). We suggest that these exceptional properties are due to a recent occurrence of the last major merger. In fact, most of them are expected to occur 6.5 to 8 Gyr ago in massive spirals (see e.g., Hammer et al. 2009a; Puech et al. 2012), instead of less than 4.6 Gyr for NGC 4013. At later time one may expect fainter loops, less intense warp, and less exceptional IR properties as the remnant is progressively relaxing. The loop redness may also support a quite recent event, because it would let enough time for the progenitors to be metal-enriched. In fact, there is still an important evolution of metal abundances during the past 6 Gyr (Rodrigues et al. 2008).

Interestingly, we find that NGC 4013, M31 and NGC 5907 would follow an order of increasing elapsed time since the last merger occurrence, i.e., 2.7-4.6, 5.5 and $\geqslant$ 6 Gyr, respectively. Kormendy et al. (2010) have investigated the R=8 Mpc volume and have shown that 11 among 19 galaxies possess a pseudo-bulge. They argued that such structures evidence a secular evolution for most spiral galaxies. At distances of 16.9 and 14 Mpc, respectively, NGC 4013 and NGC 5907 are not in the volume studied by Kormendy et al. (2010), but their properties should be similar. Both show pseudo-bulges that can be reproduced by gas-rich major mergers. As discussed in Hammer et al. (2012) while a classical bulge has to be formed through a violent event such as a major merger, a pseudo bulge does not permit to do such a distinction. In their realization of several orbits and feedback histories, they do find that most gas-rich merger remnants possess pseudo-bulges, a property confirmed by independent simulations (Keselman & Nusser 2012).

Only a major merger can reproduce all the very particular properties of NGC 4013, which places this galaxy as a potential missing link between well relaxed spiral galaxies and $\sim$ 0.5-1 Gyr post-merger galaxies such as J033245.11-274724.0 at z=0.43, which dusty forming disk makes it an excellent candidate for an early rebuilding disk phase (Hammer et al. 2009b). Further investigations would be helpful to verify the above. In fact, our model helps to predict many features (see Figure 1) that could be tested in the near future:

- Deeper observations should reveal many other loops at fainter surface-brightness levels; if obtained in two filters, color may also helps to identified the X-shaped feature in the halo as well as more accurate photometry would help to better constrain the age/metal of the stellar population;
- Deeper HI observations would provide an incomparable test between mergers of different mass ratios;

• The warp duration time (less than 2 Gyr, see bottom panels of Figure 1) could be verified by estimating the ages of the stars as done by Radburn-Smith et al. (2014) for the NGC 4565 HI disk warp;

• On average the disk stars are predicted to be of intermediate ages, i.e., formed 2.7 to 4.6 Gyr after the merger, which could be identified through the signatures of the Balmer absorption lines and the 4000A break[2].

As a concluding remark, we notice that NGC 4013 may provide a crucial test about the long-standing issue of the origin of strong warps in isolated galaxies. The observed spatial decoupling between the warp and the tidal stellar stream is supporting a major merger origin, and this alternative should be considered by future studies.

ACKNOWLEDGMENTS

We thank the referee for very useful suggestions that help to improve the paper. This work has been supported by the "Laboratoire International Associé" Origins, the Young Researcher Grant of National Astronomical Observatories, Chinese Academy of Sciences. Computations were done using the special supercomputer at the Center of Information and Computing at National Astronomical Observatories, Chinese Academy of Sciences. The images in gas surface density of Fig.1 and Fig.3 were produced using SPLASH (Price 2007).

REFERENCES

Athanassoula, E., & Misiriotis, A. 2002, MNRAS, 330, 35
Barnes, J. E., & Hernquist, L. 1992, ARA&A, 30, 705
Barway, S., Mayya, Y. D., Kembhavi, A. K., Pandey, S. K., 2005, AJ, 129, 630
Bell, E. F., McIntosh, D. H., Katz, N., & Weinberg, M. D. 2003, ApJS, 149, 289
Bottema, R., Shostak, G. S., & van der Kruit, P. C. 1987, Nature, 328, 401
Bottema, R. 1996, A&A, 306, 345
Bottema, R. 1995, A&A, 295, 605
Binney, J., & Petrou, M. 1985, MNRAS, 214, 449
Bianchi, S. 2007, A&A, 471, 765
Buta, R. J., Corwin, H. G., & Odewahn, S. C. 2007, The de Vaucouleurs Altlas of Galaxies, edited by Ronald J. Buta, Harold G. Corwin and Stephen C. Odewahn. ISBN-13 978-521-82048-6 (HB). Published by Cambridge University Press, Cambridge, UK, 2007.
Cox, T. J., Jonsson, P., Primack, J. R., & Somerville, R. S. 2006, MNRAS, 373, 1013
Comerón, S., Elmegreen, B. G., Knapen, J. H., et al. 2011, ApJL, 738, L17
Eskew, M., Zaritsky, D., & Meidt, S. 2012, AJ, 143, 139
Franx, M., van Dokkum, P. G., Schreiber, N. M. F., et al. 2008, ApJ, 688, 770
Fukugita, M.; Shimasaku, K.; Ichikawa, T., PASP, 107, 945
Hammer, F., Flores, H., Elbaz, D., Zheng, X. Z., Liang, Y. C., & Cesarsky, C. 2005, A&A, 430, 115
Hammer, F., Puech, M., Chemin, L. et al., 2007, ApJ, 662, 322
Hammer, F., Flores, H., Puech, M., Yang, Y. B., Athanassoula, E., Rodrigues, M., & Delgado, R. 2009a, A&A, 507, 1313
Hammer, F., Flores, H.; Yang, Y. B.; Athanassoula, E.; Puech, M.; Rodrigues, M.; Peirani, S. 2009b, A&A, 496, 381
Hammer, F., Yang, Y. B., Wang, J. L., Puech, M., Flores, H., & Fouquet, S. 2010, ApJ, 725, 542
Hammer, F., Flores, H. and Puech, M., 2012, Modern Physics Letters A, 33, 1230034 (arXiv:1110.1376)
Hammer, F., Yang, Fouquet, S. et al., 2013, MNRAS, 431, 3543
Hopkins, P. F., Cox, T. J., Younger, J. D., & Hernquist, L. 2009, ApJ, 691, 1168
Hopkins, P. F., Bundy, K., Croton, D. et al., 2010, ApJ, 715, 202
Hurley-Keller, D., Mateo, M., Grebel, E. K., 1999, ApJ, 523, 25
Just, A., Möllenhoff, C., & Borch, A. 2006, A&A, 459, 703
Katz, N., Weinberg, D. H., & Hernquist, L. 1996, ApJS, 105, 19
Kennicutt, R. C., Jr. 1998, ApJ, 498, 541
Keselman, J. A., Nusser, A., 2012, MNRAS, 424, 1232
Khochfar, S., & Burkert, A. 2006, A&A, 445, 403
Kormendy, J., & Kennicutt, R. C., Jr. 2004, ARA&A, 42, 603
Kormendy, J., Drory, N., Bender, R. Cornell, M. E., 2010, ApJ, 723, 54
Gomez de Castro, A. I., & Garcia-Burillo, S. 1997, A&A, 322, 381
McDonald, M., Courteau, S., & Tully, R. B. 2009, MNRAS, 393, 628
Martínez-Delgado, D., Alonso-Garca, J.; Aparicio, A., Gmez-Flechoso, M. A., 2001, ApJ, 549, 63
Martínez-Delgado, D., Gmez-Flechoso, M. ., Aparicio, A., Carrera, R., 2004, ApJ, 601, 242
Martínez-Delgado, D., Peñarrubia, J., Gabany, R. J., Trujillo, I., Majewski, S. R., & Pohlen, M. 2008, ApJ, 689, 184
Martínez-Delgado, D., Pohlen, M., Gabany, R. J., et al. 2009, ApJ, 692, 955 (M09)
Martínez-Delgado, D., Gabany, R. J., Crawford, K., et al. 2010, AJ, 140, 962
Meidt, S. E., Schinnerer, E., van de Ven, G., et al. 2014, ApJ, 788, 144
McGaugh, S. S. 2005, ApJ, 632, 859
Mouhcine, M., Bamford, S. P., Aragón-Salamanca, A., Nakamura, O., & Milvang-Jensen, B. 2006, MNRAS, 369, 891
Peng, C. Y., Ho, L. C., Impey, C. D., & Rix, H.-W. 2010, AJ, 139, 2097
Price, D. J. 2007, PASA, 24, 159
Puech, M., Hammer, F., Flores, H., et al. 2010, A&A, 510, A68
Puech, M., Hammer, F., Hopkins, P. F., et al. 2012, ApJ, 753, 128
Purcell, C. W., Bullock, J. S., Kazantzidis, S. 2010, MNRAS, 404, 1711
Radburn-Smith, D. J., de Jong, Roelof S., Streich, D. et al., 2014, ApJ, 78, 105
Read, J. I., Lake, G., Agertz, O., & Debattista, V. P. 2008, MNRAS, 389, 1041
Robertson, B., Bullock, J. S., Cox, T. J., Di Matteo, T., Hernquist, L., Springel, V., & Yoshida, N. 2006, ApJ, 645, 986
Rodrigues, M., Hammer, F., Flores, H. et al., 2008, A&A, 492, 371
Rodrigues, M., Puech, M., Hammer, F., Rothberg, B., Flores, H., 2012, MNRAS 421, 2888
Saha, K., de Jong, R., & Holwerda, B. 2009, MNRAS, 396, 409
Sheth, K., Regan, M., Hinz, J. L., et al. 2010, PASP, 122, 1397

[2] We recovered a spectrum of NGC 4013 from the SDSS, showing a quite prominent $H\delta$ absorption line, though it only covers the central part of the galaxy

Springel, V., & White, S. D. M. 1999, MNRAS, 307, 162
Springel, V. 2000, MNRAS, 312, 859
Springel, V., & Hernquist, L. 2003, MNRAS, 339, 289
Springel, V., & Hernquist, L. 2005, ApJL, 622, L9
Springel, V. 2005, MNRAS, 364, 1105
Toomre, A., & Toomre, J. 1972, ApJ, 178, 623
van der Kruit, P. C., & Searle, L. 1982, A&A, 110, 61
van der Wel, A., Franx, M., van Dokkum, P. G., et al. 2014, ApJ, 788, 28
Verstappen, J., Fritz, J., Baes, M., et al. 2013, A&A, 556, A54
Wang, J., Hammer, F., Athanassoula, E., et al. 2012, A&A, 538, A121 (Wang12)
Willick, J. A., Courteau, S., Faber, S. M., et al. 1997, ApJS, 109, 333
Wuyts, S., Cox, T. J., Hayward, C. C., et al. 2010, ApJ, 722, 1666
Zibetti, S., White, S. D. M., & Brinkmann, J. 2004, MNRAS, 347, 556